# Computationally Efficient Methods for Improved Double-Ended Transmission Line Fault Locating

Kanchanrao Dase and Normann Fischer
*Schweitzer Engineering Laboratories, Inc.*

# Computationally Efficient Methods for Improved Double-Ended Transmission Line Fault Locating

Kanchanrao Dase and Normann Fischer, *Schweitzer Engineering Laboratories, Inc.*

*Abstract*—This paper describes two different categories of impedance-based double-ended fault-locating methods used in transmission systems. The first category includes methods that use local currents and voltages and only remote currents. The second category includes methods that use both local and remote currents and voltages. This paper analyzes the accuracy and limitations of known time-synchronized double-ended fault-locating methods and proposes two new methods. These new methods are computationally efficient and improve transmission-line fault locating.

In long overhead lines or in underground cables, the shunt capacitance draws sufficient current to affect the accuracy of the fault location estimation when traditional impedance-based fault-locating equations are used. Using the $\pi$ equivalent model, we can take shunt capacitances into consideration; however, this paper illustrates why this model is not adequate for estimating fault locations. Instead, considering the distributed nature of the transmission line gives more accurate fault-locating results. The equations to model the distributed nature of transmission lines include complex hyperbolic or exponential terms, as do the fault-locating equations, making them computationally inefficient. For this reason, this approach has not been considered for real-time applications.

This paper derives computationally efficient expressions for estimating fault locations that are suitable for implementation in digital protective relays. The complex hyperbolic or the exponential terms are precalculated based on the line parameters and are used as constants when the fault-locating algorithm is triggered. The new proposed methods have significantly higher accuracy in determining fault locations than the methods that neglect the charging current or use a lumped parameter model to account for the charging current. This paper summarizes the results for fault location estimation by using test cases obtained from Electromagnetic Transients Program (EMTP) simulations.

## I. INTRODUCTION

The synchronized double-ended fault-locating methods with local measurements and remote currents described in [1] and [2] do not consider the shunt capacitance of the line. As per [3], for short lines (<50 miles) we can ignore the effects of the shunt capacitance; however, for medium length (50 to 150 miles) and long length lines (>150 miles), we should consider shunt capacitances, which can be modeled as lumped or distributed elements.

Depending on the type of fault-locating method, the shunt capacitance effects can be reduced or eliminated. Some relays use the $\pi$ transmission line model and compensate for the capacitance currents at local and remote ends. The $\pi$ equivalent model for long transmission lines can also be used [3] [4]. However, when using this method, it is difficult to accurately estimate the shunt capacitance current compensation under fault conditions because the voltage profile is no longer flat (as it is during steady-state conditions). Instead, we can inherently consider shunt capacitances in the transmission line equations with the use of the distributed line model. In this paper, we analyze the root causes affecting the accuracy of estimated fault location and propose a new computationally efficient algorithm.

For the double-ended fault-locating method with local and remote voltages and currents, [5] describes the impedance-based fault locating method based only on negative-sequence networks. Because the negative-sequence voltages are less than the positive-sequence voltages, [5] assumes the impact of negative-sequence capacitance currents to be negligible. However, this paper illustrates that ignoring capacitance can create errors in the fault location estimation, especially with lines that have high total shunt capacitances.

Reference [6] uses long transmission line equations to determine the fault location. With the use of the distributed line model, the equations inherently consider shunt capacitances. However, the algorithm comprises computation of complex hyperbolic terms for all the samples in the fault window. This may not be efficient to run in a digital relay. This paper proposes an efficient algorithm that does not require computation of complex hyperbolic terms in run time.

All the simulation results presented in this paper are for an A-phase-to-ground fault with fault resistance, $R_f = 10 \ \Omega$, unless specified otherwise. Although the proposed equations for fault locating described in this paper are for A-phase-to-ground fault, with slight modification, we can apply them to different types of faults. We use ATPDraw for modeling the two-machine system; the details of which are in the appendix. We consider a transmission line of 300 miles with transposition cycle length of 30 miles. We model a shunt reactor at the end of the line to compensate for 40 percent of the positive-sequence susceptance of the line. The proposed methods for fault locating have no implications on transmission lines with shunt reactors if the reactor's currents are subtracted from its respective line currents. All the methods analyzed and described assume that this subtraction takes place.

## II. DOUBLE-ENDED FAULT-LOCATING METHODS WITH LOCAL MEASUREMENTS AND REMOTE CURRENTS

Consider a simplified single-line representation of a transmission line which ignores shunt capacitances with a single line-to-ground (SLG) fault, as shown in Fig. 1. The fault

location for such faults is estimated by equating the faulted phase voltage to the sum of the voltage drop of that phase from the relay to the fault point and the voltage at the fault point [1].

$$V_L = V_{LF} + V_F \quad (1)$$

In terms of total fault current ($I_F$) through the fault resistance ($R_F$), (1) can be written as:

$$V_L = V_{LF} + I_F R_F \quad (2)$$

Because the fault resistance ($R_F$) is not known, it is eliminated by multiplying both the sides of (2) by the conjugate of the estimated fault current ($I_{F\_est}{}^*$). By equating imaginary parts on both sides, we get:

$$\text{Im}[V_L I_{F\_est}{}^*] = \text{Im}[V_{LF} I_{F\_est}{}^* + I_F R_F I_{F\_est}{}^*] \quad (3)$$

Ideally, $\text{Im}[I_F R_F I_{F\_est}{}^*] = 0$,

$$\text{Im}[V_L I_{F\_est}{}^*] = \text{Im}[V_{LF} I_{F\_est}{}^*] \quad (4)$$
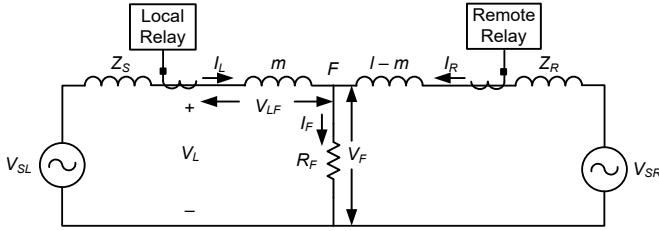


Fig. 1. Simplified single-line representation of a transmission system with an SLG fault.

For eliminating the fault resistance from (2), it is not necessary to use $I_{F\_est}{}^*$ as a multiplying factor; any phasor that has a conjugate angle of the total fault current angle can be used.

By solving (3), we can determine the accurate fault location provided that the following are true:

- The voltage drop from the relay to the fault point ($V_{LF}$) is calculated accurately and
- The fault current angle ($\angle I_{F\_est}$) is estimated accurately

Subsections A and B evaluate these two constraints through known methods.

### A. Traditional Takagi Method

#### 1) Accuracy of a Calculated Voltage Drop From the Relay to Fault Point

The traditional Takagi method ignores the shunt capacitance of the line. In this method, the relay-to-fault point voltage drop in terms of sequence currents and sequence impedances is given as follows [7].

$$V_{Relay\text{-}Fault} = mZ_{1L}\left[(I_{1L} + I_{2L} + I_{0L}) + \left(\frac{Z_{0L} - Z_{1L}}{Z_{1L}}\right)(I_{0L})\right] \quad (5)$$

where:

$Z_{1L}$ is the positive-sequence impedance of the line-per-unit length.

$Z_{0L}$ is the zero-sequence impedance of the line-per-unit length.

$m$ is the fault location from the local relay in miles or kilometers.

Equation (5) holds true if the sequence currents measured by the relay are the same until the fault point. As shown in Fig. 2, currents that result from the shunt capacitance elements of the line would be subtracted from the sequence currents measured by the relay. However, because this method completely ignores shunt capacitance, the relay introduces error in the estimation of the voltage drop from the relay to the fault point when using (5).
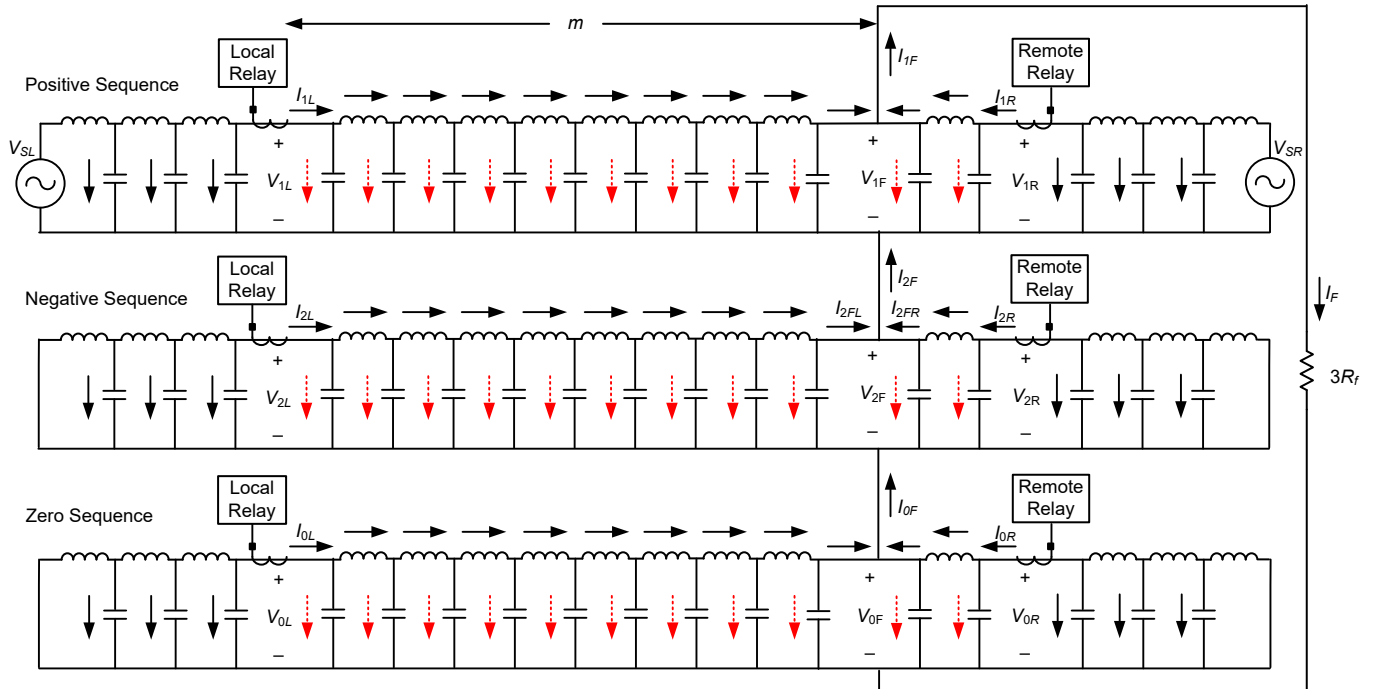


Fig. 2. Detail sequence domain network for an SLG fault.

Faults that are near to the relay do not have much difference between sequence currents measured by the relay and those going into the fault. For such faults, we can expect less error in estimating the voltage drop. The same can be seen from simulation results in Fig. 3. The error in the magnitude of the voltage drop increases drastically for fault locations beyond 100 miles, and the shunt capacitance effect becomes noticeable.
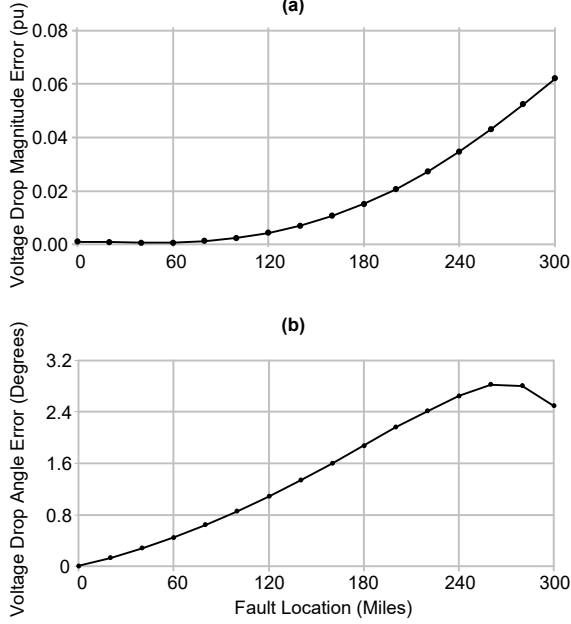


Fig. 3. Estimated voltage drop from relay-to-fault point for the traditional Takagi method: (a) magnitude error and (b) angle error.

### 2) Accuracy of the Estimated Fault Current Angle

In the traditional Takagi method, to estimate the fault current angle, we use differential negative-sequence current [8]. Fig. 2 illustrates that the negative-sequence current measured at the local and remote relays ($I_{2L}$ and $I_{2R}$) is not the same as the currents flowing into the fault ($I_{2FL}$ and $I_{2FR}$) because of the shunt capacitances. However, with some assumptions there can be almost no angle difference between the total fault current and the differential negative-sequence current, as explained later.

Consider a negative-sequence network for an unbalanced fault, as shown in Fig. 4. Let the local negative-sequence source impedance be $\overline{Z_{2S}}$ and the negative-sequence shunt capacitance impedance-per-mile be $\overline{Z_{Cap2}}$.
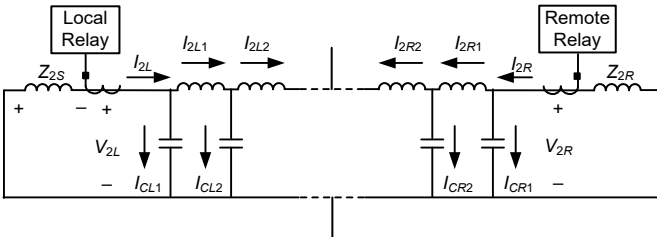


Fig. 4. Negative-sequence network for an unbalanced fault.

Assuming certain values for the parameters in Fig. 4,

$$\overline{I_{2L}} = \left|I_{2L}\right|\angle\delta, \ \overline{Z_{2S}} = \left|Z_{2S}\right|\angle 88^\circ, \ \overline{Z_{Cap2}} = \left|Z_{Cap2}\right|\angle -90^\circ$$

Because the source impedance angle is close to 90° (88° in this case) and the magnitude of the negative sequence shunt capacitance impedance-per-mile ($|Z_{Cap2}|$) for overhead lines is very high (~100–150 kΩ), the magnitude of the current through the shunt-capacitance element ($|I_{CL1}|$) would be low and would almost be in phase with the incoming negative-sequence current ($I_{2L}$), as expressed by (6). The low-magnitude shunt-capacitance element current ($I_{CL1}$), which is almost in phase with the much larger negative-sequence current ($I_{2L}$), would make little difference in the angles between $I_{2L}$ and $I_{2L1}$.

$$\overline{I_{CL1}} = \frac{\overline{V_{2L}}}{\overline{Z_{Cap2}}} = \frac{-\left|I_{2L}\right|\left|Z_{2S}\right|\angle(\delta+88^\circ)}{\left|Z_{Cap2}\right|\angle -90^\circ} \approx \frac{\left|I_{2L}\right|\left|Z_{2S}\right|}{\left|Z_{Cap2}\right|}\angle\delta \quad (6)$$

The same is true for remote-end shunt-capacitance current if the remote-source impedance angle is close to 90°. Similarly, the currents in the next shunt-capacitance elements from local and remote ends ($I_{CL2}$ and $I_{CR2}$) are in phase with the incoming currents ($I_{2L1}$ and $I_{2R1}$) provided that the negative-sequence transmission-line angle is close to 90°. Thus, if the negative-sequence impedance angles of line, local, and remote sources are close to 90°, the differential negative-sequence current angle and the total fault current angle would almost be the same, although there would be differences in their magnitudes. However, this kind of system configuration is not always practical. For a nonhomogeneous system, we can expect more error in the estimation of the fault current angle, which might result in significant error in the estimated fault location. Fig. 5 illustrates the simulation results for the difference between the differential negative-sequence current ($3I_{2L} + 3I_{2R}$) and the total fault current for homogeneous and nonhomogeneous systems.
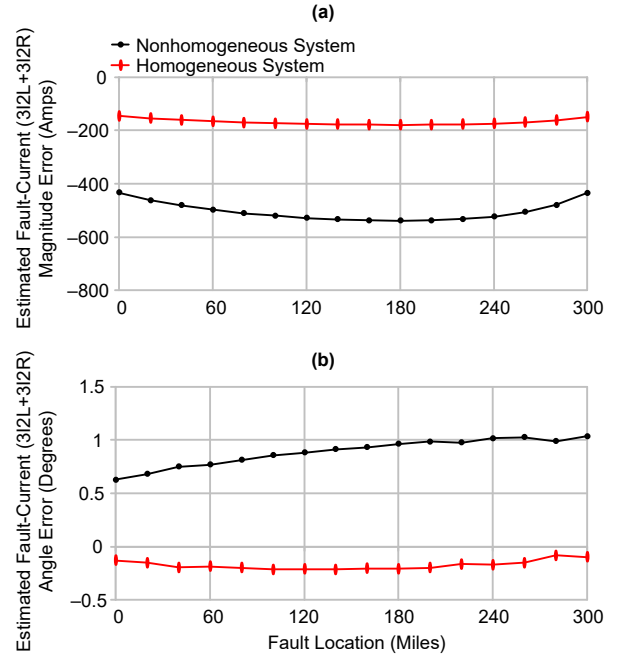


Fig. 5. Estimated magnitude and angle error of the fault current for the traditional Takagi method: (a) magnitude error and (b) angle error.

For a homogeneous system, we consider (7).

$$\angle Z_{Line} = 88.13°, \; \angle Z_{2S} = \angle Z_{2R} = 88° \quad (7)$$

For a nonhomogeneous system, we consider (8).

$$\angle Z_{2S} = 84°, \; \angle Z_{Line} = 88.13°, \; \angle Z_{2R} = 65° \quad (8)$$

### 3) Accuracy of Fault Locating

In the traditional Takagi method, the error in calculating the voltage drop from the relay to the fault point is noticeable for fault locations greater than 100 miles, as illustrated in Fig. 3. For a nonhomogeneous system, the estimated fault current angle may have errors up to a degree or more. As expected, these errors are reflected in the calculated fault location, as seen in Fig. 6.
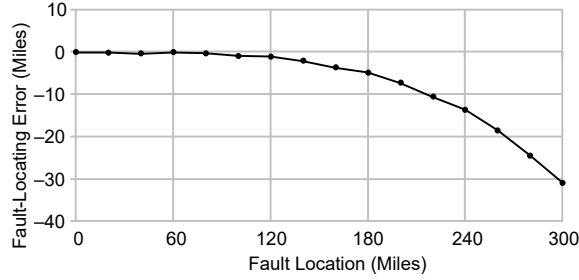


Fig. 6. Fault-locating errors by using the traditional Takagi method in a nonhomogeneous system.

### B. Takagi Method With Shunt-Capacitance Current Compensation

For medium to long overhead lines, there is adequate standing differential current under steady-state conditions because of the shunt capacitance, which might trigger sensitive differential elements; thus, this capacitance current needs to be compensated. Some relays compensate it by subtracting the estimated capacitance currents by using the π equivalent model from the measured currents at local and remote ends. See Fig. 7 for this representation. The shunt conductance (G) is assumed to be negligible and is therefore ignored.
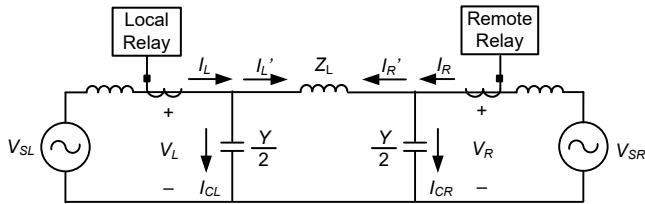


Fig. 7. Single-line representation of a π equivalent transmission system.

As shown in Fig. 8, under steady-state conditions, we can assume phase voltages at 1 pu along the line. The solid red arrows represent the actual shunt-capacitance charging currents from the local side up to half the length of the line, whereas the dashed green arrows represent the same from the remote side. The voltage angle might change along the line because of load flow, which might introduce small errors in the estimation of shunt capacitance currents at both the terminals, but most of the actual shunt-capacitance current of the line would be compensated.
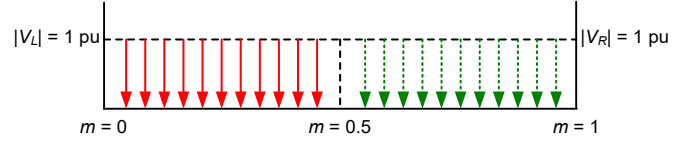


Fig. 8. Illustration of voltages and shunt-capacitance currents under steady-state conditions from local and remote terminals in the phase domain.

The differential current after compensation under steady-state conditions would be approximately zero, as shown in (9).

$$I_{DIFF} = \left( I_L{}' + I_R{}' \right) = \left[ \left( I_L - I_{CL} \right) + \left( I_R - I_{CR} \right) \right] \approx 0 \quad (9)$$

### 1) Accuracy of the Calculated Voltage Drop From the Relay to the Fault Point

Under fault conditions, the local and remote faulted-phase voltage profiles are not flat throughout the line. See Fig. 9 for this representation of a bolted SLG fault at 0.3 pu of the line length. The solid red triangle represents the actual capacitance current to be compensated in the faulted phase, whereas the solid red arrows represent the estimated charging current compensated from the local side. The estimated compensation is clearly greater than what should have been compensated for. This results in erroneously estimating the faulted-phase voltage drop from the relay to the fault point when using (10).

$$V_{Relay\text{-}Fault} = m Z_{1L} \left[ I_L{}' + \left( \frac{Z_{0L} - Z_{1L}}{Z_{1L}} \right) \left( I_{0L}{}' \right) \right] \quad (10)$$

where:

$I_L'$ is the compensated faulted-phase current at the local relay.

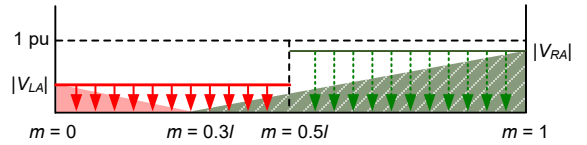$I_{0L}'$ is the compensated zero-sequence current at the local relay.



Fig. 9. Illustration of voltages and shunt-capacitance currents from local and remote terminals for a bolted SLG fault at 0.3 pu in the phase domain.

We can expect that if the fault is closer to the relay with low fault resistances, the faulted-phase voltage at the relay would be low. Thus, the actual and the estimated capacitance currents from that end would also be low enough that there would be negligible difference between them. In such cases, the voltage drop from the relay to the fault point estimated using (10) would mostly be accurate. On the other hand, if the fault is farther away from the relay, or if the fault resistance is such that the faulted-phase voltage at the relay does not drop much, there would be noticeable difference between the actual capacitance current and the estimated ones, thus erroneously estimating the faulted-phase voltage drop from the relay to the fault point. Voltage-drop errors from using the π equivalent model of the transmission line are shown in Fig. 10.
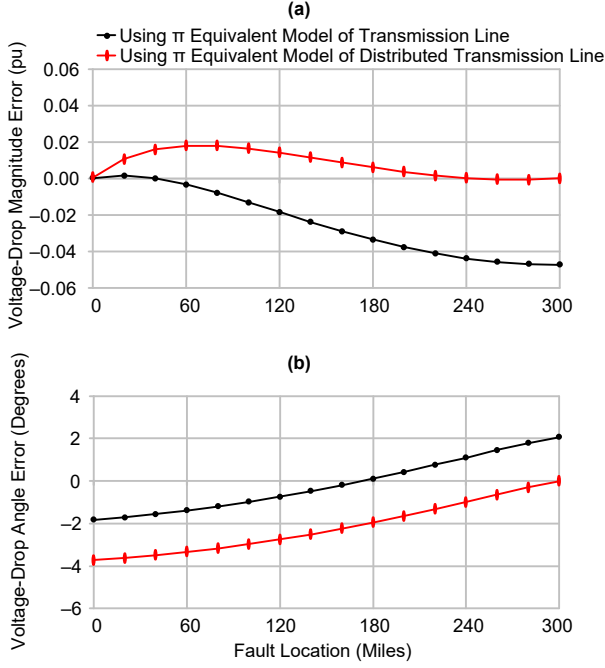
Fig. 10. Estimated voltage drop from the relay to the fault point by using the π equivalent of transmission line and distributed transmission line models: (a) magnitude error and (b) angle error.

As per [4], for long transmission lines under steady-state conditions, we should use the modified π equivalent model. The line parameters are corrected to $Z_L'$ and $Y'$, which are functions of the line propagation constant ($\gamma = \sqrt{Z_L 'Y'}$), defined as [3].

$$Z_L' = Z_L \left( \frac{\sinh \gamma l}{\gamma l} \right) \tag{11}$$

$$\frac{Y'}{2} = \frac{Y}{2} \left( \frac{\tanh \dfrac{\gamma l}{2}}{\dfrac{\gamma l}{2}} \right) \tag{12}$$

Under the fault conditions illustrated in Fig. 9, even if the line is modeled as π equivalent of the distributed transmission line, the estimated charging currents would still have errors compared to the actual charging currents for the same reasons previously explained. However, as $Z_{1L}$ and $Z_{0L}$ in (10) would be reduced using (11) by the factors $\left( \dfrac{\sinh \gamma_1 l}{\gamma_1 l} \right)$ and $\left( \dfrac{\sinh \gamma_0 l}{\gamma_0 l} \right)$ respectively, the error of the voltage drop from the relay to the fault point would be reduced. The voltage error would not be the same as it would have been if the line was modeled as π equivalent of transmission line (see Fig. 10 for details).

### 2) Accuracy of the Estimated Fault Current Angle

As in the traditional Takagi method, this version of the Takagi method with shunt-capacitance current compensation uses differential negative-sequence current for estimating the fault-current angle. The only difference is that this current is

compensated for the shunt-capacitance currents from both ends. As explained in Section II.A.2, for a homogeneous system with source impedance angles and a transmission line angle close to 90°, the differential negative-sequence current angle would be almost the same as the fault-current angle. This is because the compensated negative-sequence capacitance currents would almost be in phase with the negative-sequence currents measured by the relay. However, this is not true for a nonhomogeneous system. See Fig. 11 for simulation results of the difference between the actual fault current and the fault current estimated using compensated differential negative-sequence current ($3I_{2DIFF}$) calculated using (13) for a nonhomogeneous system.

Interestingly, even for a nonhomogeneous system (see Fig. 11 for details), there is less error in estimating the fault current as compared to the traditional Takagi method. For illustration purpose, consider a bolted SLG fault at 0.3 pu. Fig. 12 illustrates the negative-sequence voltage profiles along with the negative-sequence shunt capacitance currents from local and remote terminals for this fault. In this method, the differential negative-sequence current is given by (13). The compensated-differential current ($I_{2DIFF}$) is calculated by subtracting the summation of the estimated capacitance currents ($I_{2CL} + I_{2CR}$) from the local and remote currents ($I_{2L} + I_{2R}$) of the negative-sequence network.

$$I_{2DIFF} = \left[ \left( I_{2L} + I_{2R} \right) - \left( I_{2CL} + I_{2CR} \right) \right] \tag{13}$$
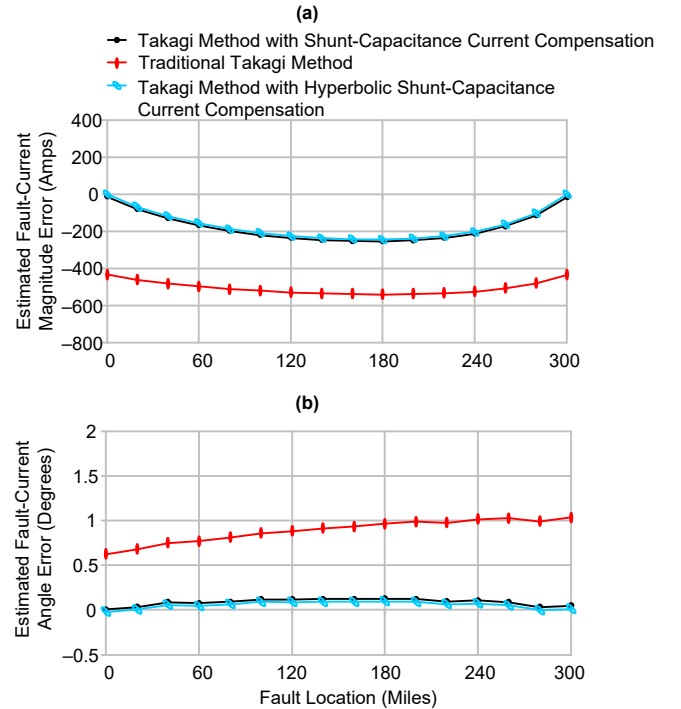


Fig. 11. Estimated fault-current angle using the traditional Takagi, shunt-capacitance compensation, and hyperbolic shunt-capacitance compensation methods for nonhomogeneous systems: (a) magnitude error and (b) angle error.
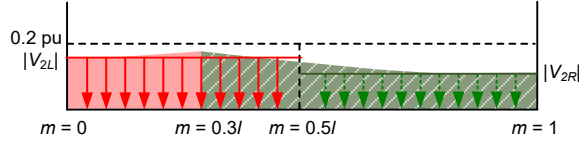
Fig. 12.　Illustration of voltages and shunt-capacitance currents from local and remote terminals for a bolted SLG fault at 0.3 pu in a negative-sequence network.

In Fig. 12, the solid red area represents the actual capacitance current from the local side whereas the red arrows represent the estimated compensated charging current. In this case, the estimation is greater than the actual charging current. On the remote side, the dashed green area represents the actual capacitance current from the remote side whereas the green arrows represent the estimated charging current compensated. In this case, the estimation is less than actual. However, in a homogeneous system, the summation of estimated capacitance currents is almost equal to the summation of actual capacitance currents from local and remote ends. Because the summation of the capacitance currents is used in (13), the calculated $I_{2DIFF}$ is almost the same as actual $I_{2DIFF}$.

In a nonhomogeneous system, under fault conditions, the local and remote negative-sequence voltage angles would be different from each other. Also, they change along the length of the line. This affects the shunt currents angle along the line. But, because the magnitudes of negative-sequence voltages are lower, the shunt currents are even lower compared to the currents flowing into the fault. Thus, the overall error in estimating fault current is less when using (13) compared to using uncompensated differential current ($I_{2L} + I_{2R}$). Simulation results show the same in Fig. 11.

### 3) Accuracy of Fault Locating

In the Takagi method with shunt-capacitance current compensation, if the line is modeled as π equivalent of the transmission line, the angle of the total fault current estimated has very low error, as seen in Fig. 11. However, the error in calculating the voltage drop from the relay to the fault point is noticeable for fault locations greater than 60 miles, as seen in Fig. 10. This error is enough to decrease the accuracy of fault locating as the distance to the fault location increases, as seen in Fig. 13. If the line is modeled as π equivalent of the distributed transmission line by using (11) and (12), the estimation of the fault current angle is almost accurate, as seen in Fig. 11. However, there are errors in the calculated voltage drop from the relay to the fault point, as seen in Fig. 10. This affects the fault-locating accuracy. Overall, we can see from Fig. 13 that there are fewer fault-locating errors using π equivalent of the distributed transmission line model than the method that uses π equivalent of the transmission line.
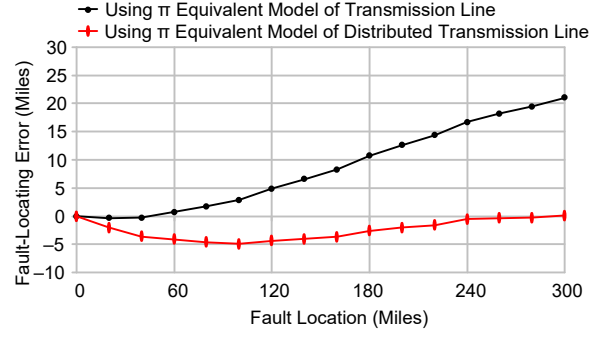


Fig. 13.　Fault locating errors from using the π equivalent of the transmission line and distributed transmission line models.

### C. Proposed Method

#### 1) Approach for Determining Accurate Fault Locating

From the two methods described in Section II, Subsections A and B, we see that the accuracy of fault locating is mostly affected by the error in the estimated voltage drop from the relay to the fault point. In the traditional Takagi method, fault locating is also affected by erroneous estimation of the fault current angle, especially in nonhomogeneous systems. The fault-current angle estimated in the Takagi method with shunt-capacitance current compensation by using the compensated differential negative-sequence current is accurate for overhead lines. The proposed method considers the root causes of errors in order to improve the accuracy of calculated fault location.

The fault voltage in sequence domain and in terms of total fault current ($I_F$) can be written as (14):

$$V_{Fault} = \left(V_{1F} + V_{2F} + V_{0F}\right) = I_F R_F \tag{14}$$

Multiplying by a conjugate of the total fault current ($I_F^*$) on both sides and taking imaginary parts, we get (15).

$$\text{Im}\left[\left(V_{1F} + V_{2F} + V_{0F}\right)I_F^*\right] = \text{Im}\left[I_F R_F I_F^*\right] = 0 \tag{15}$$

Based on Fig. 2, by using the hyperbolic equations for long transmission lines (which assumes line to be perfectly transposed) [3], we can express the fault-sequence voltages in terms of local sequence voltages and currents as follows:

$$V_{1F} = V_{1L} \cosh\left(\gamma_1 m\right) - I_{1L} Z_{C1} \sinh\left(\gamma_1 m\right) \tag{16}$$

$$V_{2F} = V_{2L} \cosh\left(\gamma_1 m\right) - I_{2L} Z_{C1} \sinh\left(\gamma_1 m\right) \tag{17}$$

$$V_{0F} = V_{0L} \cosh\left(\gamma_0 m\right) - I_{0L} Z_{C0} \sinh\left(\gamma_0 m\right) \tag{18}$$

where:

$Z_{C1}$ is the positive-sequence characteristic impedance of the line.

$Z_{C0}$ is the zero-sequence characteristic impedance of the line.

$\gamma_1$ is the positive-sequence propagation constant of the line.

$\gamma_0$ is the zero-sequence propagation constant of the line.

$m$ is the fault location from the local relay in miles or kilometers.

Similarly, based on Fig. 2, by using the hyperbolic equations, we can express the total fault current accurately in terms of negative-sequence currents at the fault point as follows.

$$I_F = 3\left(I_{2FL} + I_{2FR}\right) \quad (19)$$

where:

$$I_{2FL} = I_{2L}\cosh(\gamma_1 m) - \frac{V_{2L}}{Z_{C1}}\sinh(\gamma_1 m) \quad (20)$$

and

$$I_{2FR} = I_{2R}\cosh\left[\gamma_1(l-m)\right] - \frac{V_{2R}}{Z_{C1}}\sinh\left[\gamma_1(l-m)\right] \quad (21)$$

where:

$l$ is the total length of the line in miles or kilometers.

We see in (21) that $I_{2FR}$ uses the negative-sequence remote voltage ($V_{2R}$), but because only remote currents are available at the local relay, we cannot use (21).

Based on Fig. 2, by using the hyperbolic equations, we can express the remote negative-sequence current ($I_{2R}$) in terms of negative-sequence fault voltage ($V_{2F}$) and negative-sequence fault current from the remote side ($I_{2FR}$) as follows:

$$I_{2R} = I_{2FR}\cosh\left[\gamma_1(l-m)\right] + \frac{V_{2F}}{Z_{C1}}\sinh\left[\gamma_1(l-m)\right] \quad (22)$$

Also, applying Kirchhoff's current law at the fault point in Fig. 2, we get (23).

$$I_{2F} = I_{2FL} + I_{2FR} \quad (23)$$

Reference [6] uses (17), (20), (22), and (23) along with trigonometric identities to express $I_{2F}$ as:

$$I_{2F} = \frac{\left[I_{2L}\cosh(\gamma_1 l) - \frac{V_{2L}}{Z_{C1}}\sinh(\gamma_1 l) + I_{2R}\right]}{\cosh\left[\gamma_1(l-m)\right]} \quad (24)$$

We can use (16), (17), (18), and (24) as the variables in (15) to find the fault location ($m$). We can express this equation as (25), which is an ideal expression to determine fault location ($m$) with local measurements and remote end currents. It must be noted that fault location ($m$) is implicitly defined. You can use an iterative approach; however, it would not be computationally efficient because (25) is a multiplication of two functions of fault location ($m$). Also, any approximations or errors in hyperbolic or measured analogs would affect the fault-locating accuracy.

$$\mathrm{Im}\left\{(A+B)\left\{\frac{C}{\cosh\left[\gamma_1(l-m)\right]}\right\}^*\right\} = 0 \quad (25)$$

where:

$A$ is $(V_{1L}+V_{2L})\cosh(\gamma_1 m) - (I_{1L}+I_{2L})Z_{C1}\sinh(\gamma_1 m)$

$B$ is $V_{0L}\cosh(\gamma_0 m) - I_{0L}Z_{C0}\sinh(\gamma_0 m)$

$C$ is $I_{2L}\cosh(\gamma_1 l) - \frac{V_{2L}}{Z_{C1}}\sinh(\gamma_1 l) + I_{2R}$

As discussed in Section II.B.2, the compensated-differential negative-sequence current gives a very good estimation of the fault current angle.

$$\angle I_F \approx \angle\left(I_{2L}{}' + I_{2R}{}'\right) \quad (26)$$

Using (16), (17), (18), and (26), we can write (15) as:

$$\mathrm{Im}\left\{(A+B)\left(I_{2L}{}' + I_{2R}{}'\right)^*\right\} = 0 \quad (27)$$

We can use (27) to determine the fault location ($m$). This is also not a closed-loop solution, so we use an iterative approach. However, the expression is not as complicated as (25) and is comparatively efficient in computation.

If (27) is plotted for all values of $m$ throughout the transmission line, it would be zero exactly at the fault location provided $\left[I_{2L}{}' + I_{2R}{}'\right]$ gives the exact fault-current angle. Fig. 14 depicts the plot of the left-hand side of (27) for all values of $m$ for a bolted SLG fault at 250 miles. The plot is almost a straight line, and thus, even with two iterations, we can accurately estimate fault location. The plot is expected to bend more for higher values of shunt capacitances, such as in cables. This is because the shunt capacitance element would add its current into the line, creating more voltage drops.

The first iterative fault location obtained is close to the solution, and with the second iteration, the solution obtained would be accurate enough to be considered the fault location. For the iterative approach, we can use the Newton Raphson method as defined by (28).

$$m_2 = m_1 - \frac{f(m_1)}{f'(m_1)} \quad (28)$$

where:

$m_1$ is the initial value of the fault location.

$m_2$ is the next value of the fault location.
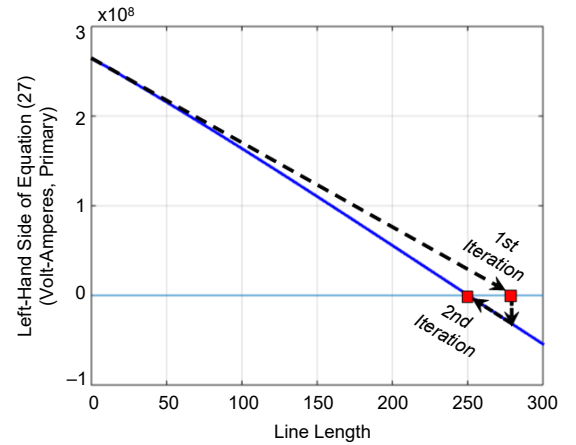
$f(m_1)$ is the left-hand side of (27) at $m_1$.



Fig. 14. Plot of the fault location equation, i.e., left-hand side of (27) for all values of $m$ for a bolted SLG fault at 250 miles.

For the first iteration, the initial value $m_1$ can be taken as 0. Thus, using (27) as $f(m_1)$ with $m_1 = 0$ in (28), the first iterative fault location solution ($FL_1$), substituting $\cosh(0) = 1$ and $\sinh(0) = 0$, would be given as follows:

$$FL_1 = \frac{\text{Im}\left[\left(V_{1L} + V_{2L} + V_{0L}\right)\left(I_{2L}' + I_{2R}'\right)^*\right]}{\text{Im}\left\{\left[\left(I_{1L} + I_{2L}\right)Z_{C1}\gamma_1 + I_{0L}Z_{C0}\gamma_0\right]\left[I_{2L}' + I_{2R}'\right]^*\right\}} \quad (29)$$

Adding and subtracting $I_{0L}Z_{C1}\gamma_1$ in the denominator of (29) and simplifying the equation by substituting $Z_{C0}\gamma_0 = Z_{L0}$ and $Z_{C1}\gamma_1 = Z_{L1}$, we get:

$$FL_1 = \frac{\text{Im}\left[V_{AL}\left(I_{2L}' + I_{2R}'\right)^*\right]}{\text{Im}\left\{\left\{Z_{L1}\left[I_{AL} + I_{0L}\left(\frac{Z_{L0} - Z_{L1}}{Z_{L0}}\right)\right]\right\}\left[I_{2L}' + I_{2R}'\right]^*\right\}} \quad (30)$$

Equation (30) is in the form of the fault-locating expression used in the traditional Takagi method. The only difference between the two is the conjugate multiplied in the numerator and denominator. In (30), the conjugate is the compensated differential negative-sequence current. The fault location, $FL_1$, given by (30) is used in the second iteration to find $FL_2$, which would be accurate enough to be considered desired fault location, as explained previously.

Because the value of the fault location obtained from the first iteration through use of (30) would be in the known range, e.g., 0 to 1.5 times the total line length, we can use a predesigned look-up table and interpolation to determine the values of the hyperbolic terms used in (31), which is the second iterative expression. With this approach, we can efficiently compute (31).

$$FL_2 = FL_1 - \frac{\text{Im}\left\{(A + B)\left(I_{2L}' + I_{2R}'\right)^*\right\}}{\text{Im}\left\{(A' + B')\left(I_{2L}' + I_{2R}'\right)^*\right\}} \quad (31)$$

where:

$A$ is $\left(V_{1L} + V_{2L}\right)\cosh\left(\gamma_1 FL_1\right) - \left(I_{1L} + I_{2L}\right)Z_{C1}\sinh\left(\gamma_1 FL_1\right)$

$B$ is $V_{0L}\cosh\left(\gamma_0 FL_1\right) - I_{0L}Z_{C0}\sinh\left(\gamma_0 FL_1\right)$

$A'$ is
$\gamma_1\left(V_{1L} + V_{2L}\right)\sinh\left(\gamma_1 FL_1\right) - \left(I_{1L} + I_{2L}\right)Z_{L1}\cosh\left(\gamma_1 FL_1\right)$

$B'$ is $\gamma_0 V_{0L}\sinh\left(\gamma_0 FL_1\right) - I_{0L}Z_{L0}\cosh\left(\gamma_0 FL_1\right)$

*2) Accuracy of Fault Locating*

As per the simulation results, fault location estimated using the proposed method has errors less than half a mile with $R_f = 10\ \Omega$. The calculated fault location also includes errors introduced by transmission line transposition. Earlier known methods (described in Section II, Subsection A and B) have larger errors, and some of them have errors in tens of miles. This is depicted in Fig. 15.
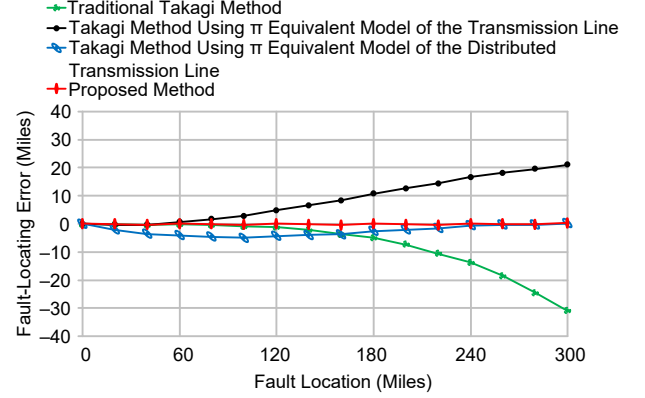


Fig. 15. Fault-locating errors for different methods for $R_f = 10\ \Omega$.

The accuracy of estimating the fault location with the proposed method may slightly decrease with increase in the fault resistance because as the fault resistance increases, the fault voltage also increases and the small angle error of the fault current determined by using (13) gets multiplied with an increased value of the fault voltage in (27). This is depicted in Fig. 16.
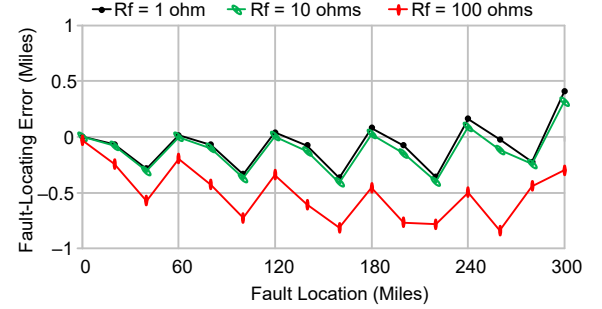


Fig. 16. Fault-locating errors from using the proposed method for different values of $R_f$.

## III. Double-Ended Fault Locating Methods With Local and Remote Currents and Voltages

The double-ended fault locating methods with two end voltages and two end currents can be more accurate than methods with two end currents and one end voltage because of the following:

- Both the end voltages and currents are known, we can only use a positive- or negative-sequence network for fault locating. The positive- or the negative-sequence parameters can be accurately known for a transmission line and are constant if the geometry of the transmission line is the same. Whereas, the zero-sequence parameters can change because of weather conditions or different zero-sequence return paths, thus decreasing the accuracy of fault location if zero-sequence parameters are involved.
- We only use a negative- or positive-sequence network, the zero-sequence mutual coupling from the parallel lines does not significantly affect the fault location estimation [5].

Subsections A, B, and C further describe the known double-ended fault-locating methods with two end voltages and two end currents.

## A. Impedance-Based Fault-Locating Method

In this method, the local relay has access to voltage and current measurements from both terminals, and the algorithm ignores shunt capacitances of the line. Given a negative-sequence network for an unbalanced fault, as shown in Fig. 17, fault location (*m*) is derived as follows.
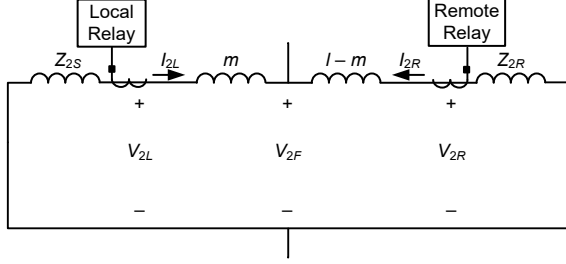


Fig. 17.   Negative-sequence network for an unbalanced fault.

Negative-sequence fault voltage ($V_{2F}$) from the local end is given by (32):

$$V_{2F} = V_{2L} - mZ_{1L}I_{2L} \qquad (32)$$

where:

$Z_{1L}$ is the positive-sequence impedance of the line per-unit length.

$m$ is the fault location from the local relay in miles or kilometers.

The negative-sequence fault voltage ($V_{2F}$) from the remote end is given by (33):

$$V_{2F} = V_{2R} - (l - m)Z_{1L}I_{2R} \qquad (33)$$

Equating (32) and (33), the fault location (*m*) comes out to (34):

$$m = \left[\frac{V_{2L} - V_{2R} + I_{2R}Z_{1L}l}{(I_{2L} + I_{2R})Z_{1L}}\right] \qquad (34)$$

Graphically, the fault location given by (34) is the point of intersection of the negative-sequence voltage profile from the local end given by (32) and the negative-sequence voltage profile from the remote end given by (33).

The negative-sequence shunt-capacitance currents can be small because the respective negative-sequence voltages are low compared to the positive-sequence voltages, but they can still impact the accuracy of fault location. This is because in the impedance-based fault-locating method, the fault location is the point of intersection of the negative-sequence voltage profiles from local and remote ends, which will not be the same if shunt capacitances are involved. These capacitance elements continue to add their current into the line, creating more voltage drop, thus bending the voltage profiles. Fig. 18 shows the local and remote negative-sequence voltage characteristics based on (32) and (33) for a fault at 30 miles in the overhead line. The point of intersection of these voltage characteristics is at 37 miles, thus giving an error of 7 miles in determining the fault location. The errors in the case of underground cables would be more because of higher values of shunt capacitances.

We can improvise the accuracy of the fault location by using (34) if we compensate the currents used in the equation for shunt-capacitance currents by using the π equivalent model of the distributed transmission line. However, there would still be error because exact capacitance current compensation requires knowledge of the fault location and the negative-sequence fault voltage ($V_{2F}$), both of which are unknown. Fig. 19 illustrates fault-locating errors for overhead line and underground cable through use of (34) with and without shunt-capacitance current compensation.
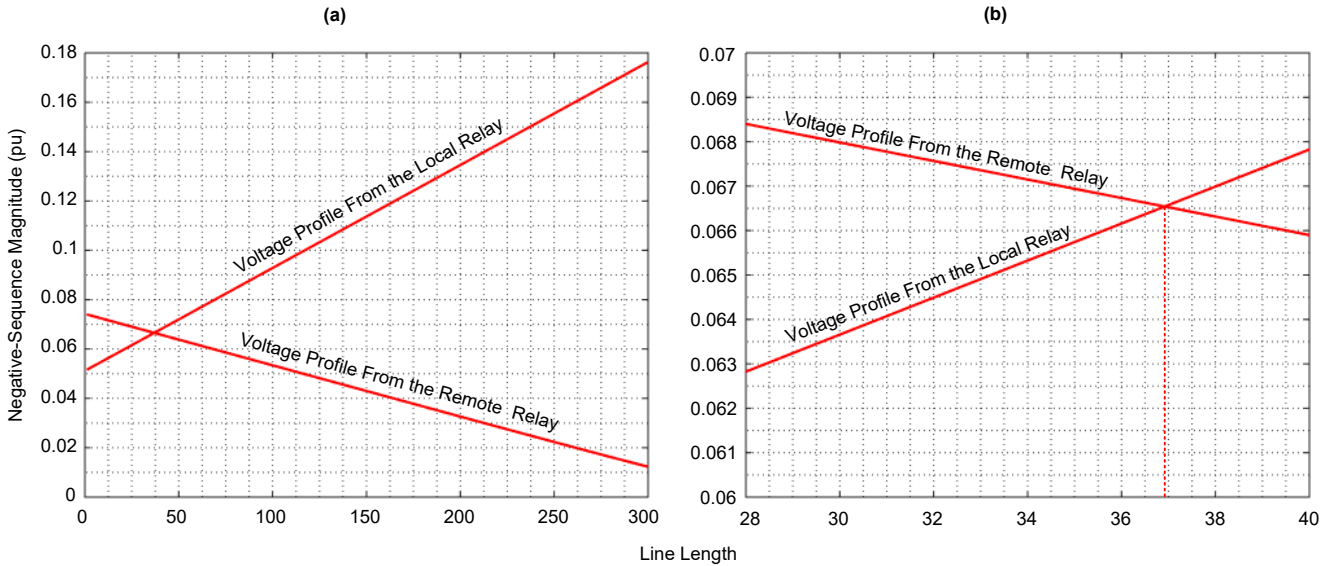


Fig. 18.   Negative-sequence voltage profiles through use of (32) and (33) for a fault at 30 miles: (a) voltage profiles throughout the line and (b) zoom-in voltage profiles.
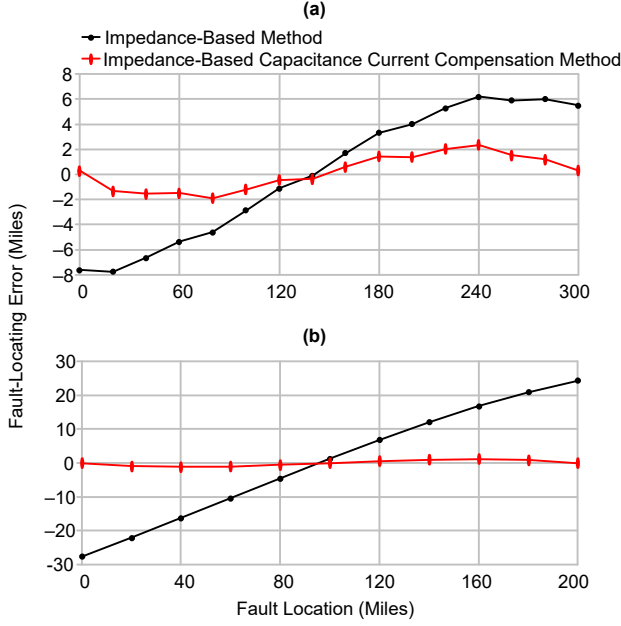
Fig. 19. Fault-locating errors for different methods for $R_f = 10\ \Omega$: (a) overhead line (300 miles, transposition cycle of 30 miles) and (b) underground cable (200 miles, perfectly transposed)

### B. Fault Locating Through Use of Distributed Transmission Line Equations in Logarithmic Form

Errors introduced by the shunt capacitances can be eliminated by using the distributed parameter transmission line equations. Fault location determined by this method is accurate because the shunt capacitances are inherently included in the equations. The following steps derive the expression for fault location ($m$).

The expression for negative-sequence fault voltage ($V_{2F}$) from the local end in exponential form is given by [3].

$$V_{2F} = \left(\frac{V_{2L} - I_{2L}Z_{C1}}{2}\right)e^{m\gamma_1} + \left(\frac{V_{2L} + I_{2L}Z_{C1}}{2}\right)e^{-m\gamma_1} \quad (35)$$

where:

$Z_{C1}$ is the positive-sequence characteristic impedance of the line.

$\gamma_1$ is the positive-sequence propagation constant of the line.

The expression for negative-sequence fault voltage ($V_{2F}$) from the remote side in exponential form is given by [3].

$$V_{2F} = \left(\frac{V_{2R} - I_{2R}Z_{C1}}{2}\right)e^{(l-m)\gamma_1} + \left(\frac{V_{2R} + I_{2R}Z_{C1}}{2}\right)e^{-(l-m)\gamma_1} \quad (36)$$

Equating (35) and (36), the expression for fault location ($m$) in logarithmic form is given as (37).

$$m = \frac{1}{\gamma_1}\ln\sqrt{\frac{\left(V_{2R} - I_{2R}Z_{C1}\right)e^{\gamma_1 l} - \left(V_{2L} + I_{2L}Z_{C1}\right)}{\left(V_{2L} - I_{2L}Z_{C1}\right) - \left(V_{2R} + I_{2R}Z_{C1}\right)e^{-\gamma_1 l}}} \quad (37)$$

### C. Fault Locating Through the Use of Distributed Transmission Line Equations in Hyperbolic Form

Because the distributed parameter transmission line equations can also be expressed in hyperbolic format, the fault location ($m$) in hyperbolic form can be derived as follows.

The expression for negative-sequence fault voltage ($V_{2F}$) from the local side in hyperbolic form is given by [3].

$$V_{2F} = V_{2L}\cosh\left(m\gamma_1\right) - I_{2L}Z_{C1}\sinh\left(m\gamma_1\right) \quad (38)$$

The expression for negative-sequence fault voltage ($V_{2F}$) from the remote side in hyperbolic form is given by [3].

$$V_{2F} = V_{2R}\cosh\left[(l-m)\gamma_1\right] - I_{2R}Z_{C1}\sinh\left[(l-m)\gamma_1\right] \quad (39)$$

Equating (38) and (39), the expression for fault location ($m$) in hyperbolic form is given as (40).

$$m = \frac{1}{\gamma_1}\tanh^{-1}\left(\frac{V_{2L} - V_{2R}\cosh\left(\gamma_1 l\right) + I_{2R}Z_{C1}\sinh\left(\gamma_1 l\right)}{I_{2L}Z_{C1} - V_{2R}\sinh\left(\gamma_1 l\right) + I_{2R}Z_{C1}\cosh\left(\gamma_1 l\right)}\right) \quad (40)$$

Equations (37) and (40) are basically the same, but they are in different mathematical forms.

Considering the same example as that given in Fig. 18, (the fault location at 30 miles), the hyperbolic negative-sequence voltage profiles from the local and remote terminals obtained through use of (38) and (39) are plotted in Fig. 20 (indicated by blue lines).

The impedance-based negative-sequence voltage profiles are also plotted using (32) and (33), indicated by red lines. Voltage profiles formed from hyperbolic equations bend slightly. This is because the shunt-capacitance elements through the line keep adding the shunt-capacitance current to the line, thus creating more voltage drop.

We can determine the fault location as the intersection of the voltage profiles by using the distributed transmission line equations instead of the impedance-based method. From Fig. 20, we can see that the point of intersection of the hyperbolic voltage profiles (i.e., the fault-locating point) is about 0.4 miles off the actual fault location, which is 30 miles. This error is because of the transmission line transposition. Fault locating with distributed transmission line equations uses complex logarithmic or inverse hyperbolic equations, and using such equations for all the samples in the fault window might not be computationally efficient. For example, one way to solve complex logarithmic or inverse tanh functions is through series expansion, as expressed in (41) and (42) [9].

$$\ln(x) = (x-1) - \frac{(x-1)^2}{2} + \frac{(x-1)^3}{3} - \frac{(x-1)^4}{4} + \frac{(x-1)^5}{5} - \frac{(x-1)^6}{6}\ldots \quad (41)$$

$$\tanh^{-1}(x) = x + \frac{x^3}{3} + \frac{x^5}{5} + \frac{x^7}{7} + \frac{x^9}{9} + \frac{x^{11}}{11}\ldots \quad (42)$$
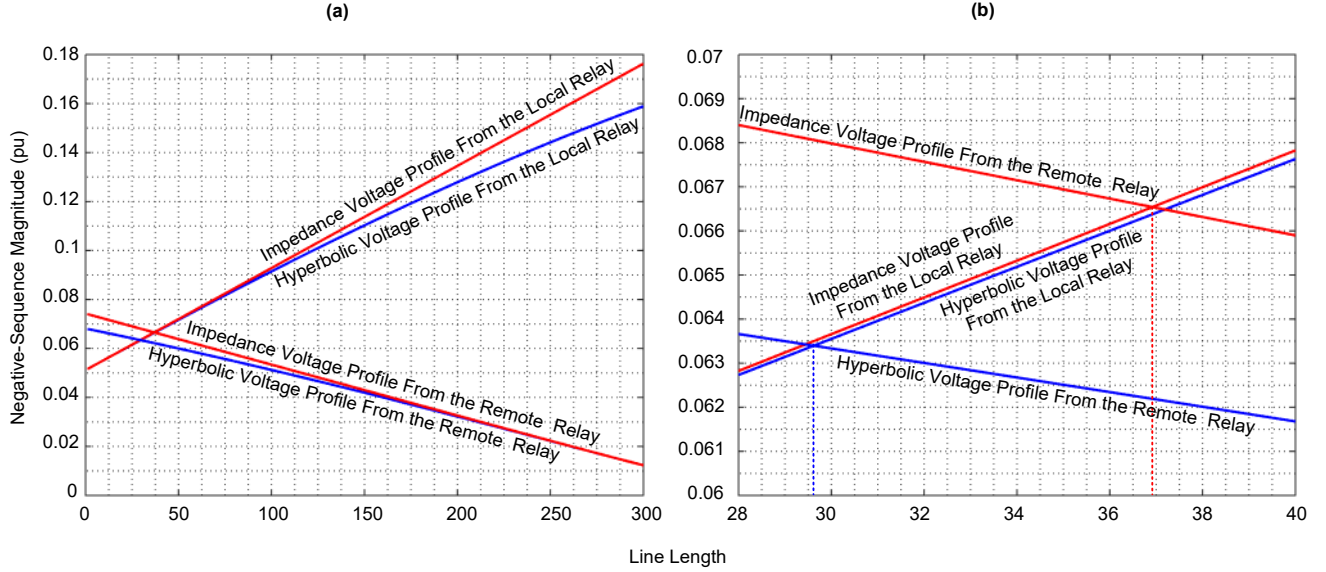
Fig. 20.   Negative-sequence voltage profiles through use of (32), (33), (38), and (39) for a fault at 30 miles: (a) voltage profiles throughout the line and (b) zoom-in voltage profiles.

Using the first six terms of the series expansions (41) and (42), the estimated fault location can be accurate with error up to a half mile. However, some fault cases might require more than the first six terms for accurate results. Also, using the above series expansions, the real-time computation would be inefficient because higher powers of complex numbers are involved for all the samples in the fault window. Thus, a computationally efficient algorithm is required, especially when run in the relay, which is explained further in Section III.D.

### D.  Computationally Efficient Algorithm

#### 1)  Introduction to the Computationally Efficient Algorithm

The proposed computationally efficient algorithm method is a two-step approach. In the first step, we calculate an approximate fault location by using negative-sequence voltage profiles. In the second step, we add a predetermined correction factor to compensate for the fault-locating error introduced in the first step. A short summary of the steps is as follows:

First, calculate the approximate fault location by using the following:

- The measured negative-sequence voltages at local and remote terminals. These are Points 1 and 2 in Fig. 21.
- The calculated virtual local and remote negative-sequence voltages by using (38) and (39), substituting $m$ with $l$ (total line length). These are Points 3 and 4 in Fig. 21.
- The approximate fault location—the point of intersection formed by the two segments (1–4 and 2–3). This is Point 5 in Fig. 21, but because it is an approximate estimated fault location, it has error.

The expression for approximate fault location is given by (43).

$$m_{approx} = \frac{l}{1 + \dfrac{V_{2L}\cosh(\gamma_1 l) - I_{2L}Z_{C1}\sinh(\gamma_1 l) - V_{2R}}{V_{2R}\cosh(\gamma_1 l) - I_{2R}Z_{C1}\sinh(\gamma_1 l) - V_{2L}}} \quad (43)$$

Second, compensate for fault-locating error in the approximate fault location obtained in the first step. Do so by adding a predetermined correction factor (explained in Section III.D.2) to the approximate fault location; the resulting corrected fault location is the final fault location declared by the algorithm.

Fig. 21 illustrates that the fault-locating error through use of (43) is negative when the actual fault location is 60 miles and positive when the actual fault location is 240 miles. This error can be as far as two miles (the error for cables can be greater because of higher shunt-capacitance values). The error is caused by the bend in the voltage profiles because of the shunt capacitances of the line and is not based on local or remote sources or its parameters. The bend in the voltage profiles is only a result of the line parameters, and it is also the only source of error between the approximate fault location (43) and actual fault location. Thus, we can determine this error by simplifying the local and remote sources. One way to do this is by assuming the same transmission line with infinite local and remote sources and then finding the fault-locating error for different fault locations. If we can calculate the error in using the approximate fault location equation (43), we can estimate an accurate fault location. We further discuss the estimation of error from using the approximate fault location equation (43) in the following section.
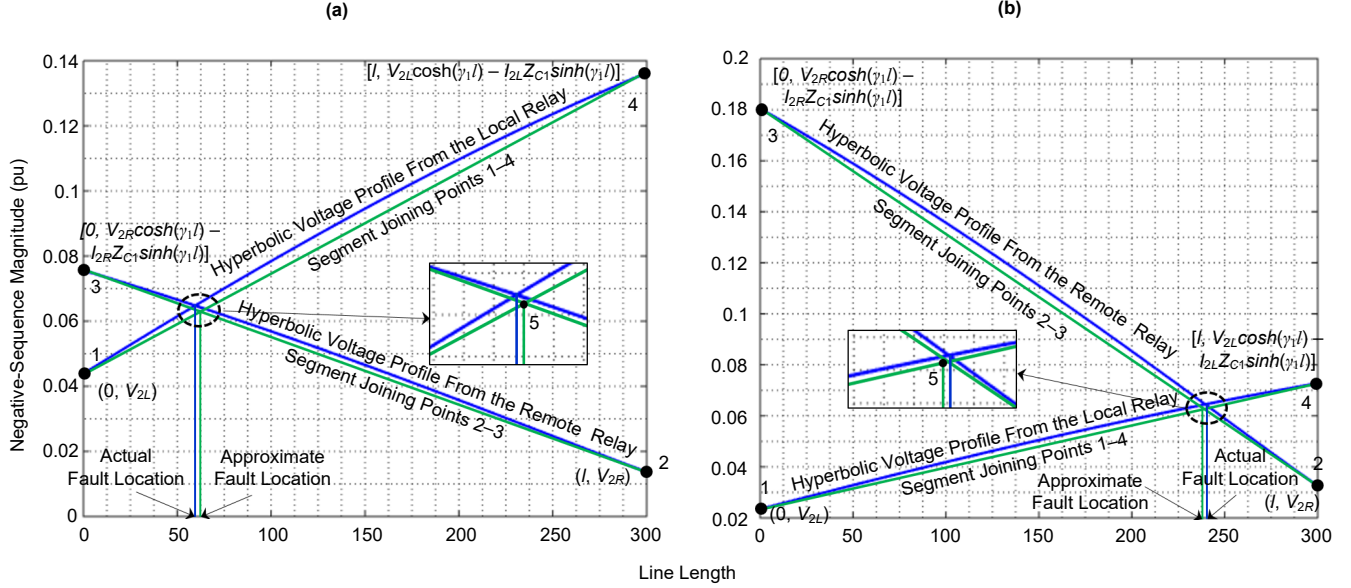
Fig. 21.  Negative-sequence voltage profiles (blue lines) by using ideal hyperbolic (or logarithmic) equations for faults at: (a) 60 miles and (b) 240 miles.

### 2) Correction Factor (Estimation of Error in Using the Approximate Fault Location Equation)

Because the error in using (43) is based on line parameters and not on source parameters, we deduce a correction factor that uses the same transmission line parameters but assumes the local and remote sources to be infinite. This makes the local and remote negative-sequence voltages zero, as shown in Fig. 22.
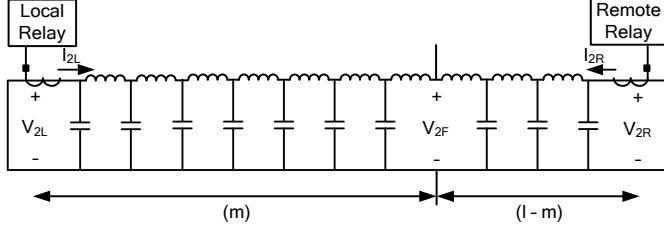


Fig. 22.  Negative-sequence network with infinite local and remote sources.

Thus, the approximate fault location equation (43) for this infinite-sources system would reduce to (44).

$$m_{approx\_infinite\_sources} = \frac{l}{1+\dfrac{I_{2L}}{I_{2R}}} \qquad (44)$$

Equating (38) and (39) (the negative-sequence fault voltages from the local and remote sides) and because $V_{2L} = V_{2R} = 0$ for this infinite-sources system, as seen in Fig. 22, we can find that,

$$\frac{I_{2L}}{I_{2R}} = \frac{\sinh\left[(l-m)\gamma_1\right]}{\sinh(\gamma_1 m)} \qquad (45)$$

Substituting (45) in (44), an approximate fault location with local and remote sources as infinite, is given by (46):

$$m_{approx\_infinite\_sources} = \frac{l}{1+\dfrac{\sinh\left[(l-m)\gamma_1\right]}{\sinh(\gamma_1 m)}} \qquad (46)$$

And the error in (46) can be expressed as follows:

$$Correction\ Factor\ \left(m_{error}\right) = m - \frac{l}{1+\dfrac{\sinh\left[(l-m)\gamma_1\right]}{\sinh(\gamma_1 m)}} \qquad (47)$$

where:

$m$ is the actual fault location from the local relay in miles or kilometers.

In other words, the correction factor in (47) is the fault-locating error for the same transmission line considered in Fig. 21 but with local and remote sources as infinite. We can precalculate the correction factor by using (47) because it is independent of currents and voltages. If we plot the correction factor by using (47) and compare it with the fault-locating error (of the same transmission line) caused in the actual system—with actual local and remote sources, i.e., the actual fault location minus the approximate fault location found in (43)—then the correction factor and fault-locating error are almost the same. Fig. 23 illustrates this.
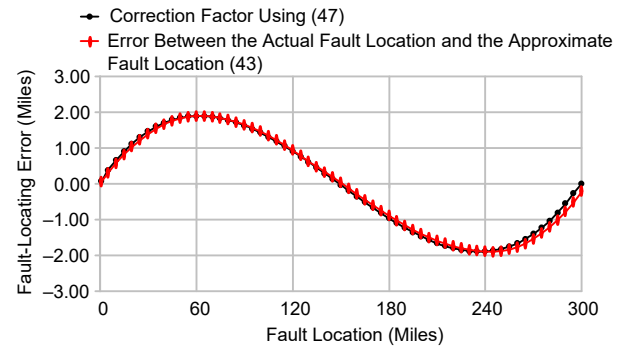


Fig. 23.  Fault-locating errors for a normal system and an infinite sources system (assuming line to be completely transposed).

So, once the approximate fault location is calculated by using (43), we add the respective correction factor (at that approximate fault location) to get the accurate fault location. This corrected fault location is given as (48):

$$m_{corrected} = m_{approx} + Correction\ Factor|_{m_{approx}} \quad (48)$$

In (48), the hyperbolic terms used in calculating the approximate fault location and the correction factor are precalculated and do not require calculation in real time. This makes the algorithm efficient enough to run in a relay.

Fig. 24 illustrates the fault-locating errors for overhead line and underground cable that were calculated by using (40) and (48). The errors seen in Fig. 24 occur because of line transposition.
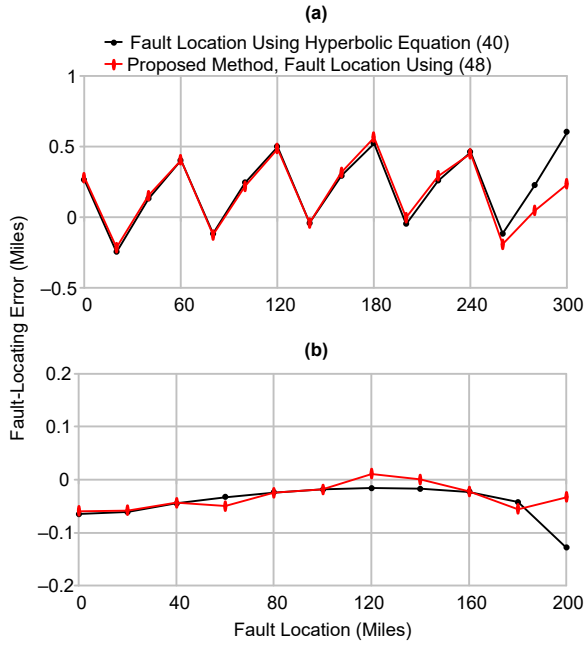


Fig. 24. Fault-locating errors for different methods for $R_f = 10\ \Omega$ (a) overhead line (300 miles, transposition cycle of 30 miles) and (b) underground cable (200 miles, perfectly transposed).

## IV. CONCLUSION

### A. Double-Ended Fault-Locating Methods With Local Measurements and Remote Currents

In the traditional Takagi method or the Takagi method with shunt-capacitance current compensation for determining fault location, the major source of error is in the estimation of voltage drop from the relay to the fault point. Also, in the traditional Takagi method, the fault-current angle can be erroneously estimated from the differential negative-sequence current, especially for systems with positive-sequence line and source impedance angles not close to 90°.

Using the compensated differential negative-sequence current, we can expect good estimation of the fault-current angle (less than a quarter degree for overhead lines). We can obtain a more accurate fault-current angle by using hyperbolic equation (24); however, the use of such expression in determining fault location iteratively is computationally inefficient.

The proposed fault-locating method does not contain any hyperbolic terms for estimating the fault-current angle. Even though the proposed method is an iterative approach, we can obtain good accuracy with just two iterations. Also, with a predefined look-up table and interpolation for hyperbolic terms that are used for calculating the fault voltage, computation becomes efficient.

Calculations of fault location through use of the traditional Takagi method are expected to be accurate for overhead transposed transmission lines as long as 100 miles. Beyond that length, the error starts increasing exponentially. With the shunt-current compensation method, the estimated fault location error increases with faults beyond 60 miles. However, with the use of the π equivalent model for distributed transmission lines, the error reduces but still can be 5 miles or more. Both of the capacitance-compensated fault-locating methods are not adequate for long transmission lines. Moreover, errors in fault location when using these methods can be worse than the plots in Fig. 15 because they are dependent on line shunt capacitances and, to some extent, on system-impedance ratios, loading conditions, fault resistance, system nonhomogeneity, and other factors.

For the proposed method, the accuracy of fault location depends only on the accuracy of the estimated fault-current angle, which depends on the fault resistance, shunt-capacitance value, and, to some extent, system nonhomogeneity. From the simulations, which assume transmission-line transposition cycle length of 30 miles, the proposed method can have fault location errors less than a half mile for low-fault resistances in nonhomogeneous systems. Though the accuracy slightly decreases for higher fault resistance, the error remains less than a mile. Whereas other methods can have larger errors, some even in tens of miles.

The proposed method would not be ideal for underground cables because the method uses zero-sequence parameters that are not accurately known for underground systems. Also, because of higher shunt-capacitance values in cables, there may be errors in the fault-current angle estimation, which would lead to errors in the calculated fault location.

The ultimate way to get accurate fault-locating estimates is by using traveling-wave fault-locating algorithms. The proposed method is a good compromise (a "middle ground") between known traditional impedance-based fault-locating methods and traveling-wave fault-locating methods. It allows us to very accurately compensate for line shunt-capacitances without requiring a global time source, like GPS, by aligning the analogs through use of channel-based synchronization.

## B. Double-Ended Fault-Locating Methods With Local and Remote Currents and Voltages

Impedance-based methods, which neglect shunt capacitance, are suitable for short overhead lines. The fault-locating errors of this method increase with the increase in the total shunt capacitance of the line. The shunt capacitances bend the negative-sequence voltage profiles by adding shunt currents into the line. Therefore, for medium or long overhead lines, this method is prone to errors. As seen in Fig. 19, error in estimating the fault location can be as long as 8 miles for a 300-mile transmission line and as long as 30 miles for a 200-mile underground cable.

If the negative-sequence currents used in the impedance-based method (34) are compensated for shunt-capacitance currents by using the π equivalent model of the distributed transmission line, the errors in the estimated fault location can come down to less than 3 miles for both long overhead lines and underground cables. However, the errors can get larger because they depend on the correct compensation of shunt-capacitance currents under fault conditions. For correct compensation, we need exact fault location and negative- (or positive-) sequence fault voltages, both of which are unknown.

The logarithmic or hyperbolic form of estimating fault location by using (37) or (40) can be accurate. We can use the respective series-expansion forms (41) and (42) for estimating fault location. The errors can be as large as a half mile, but in most fault cases, the equations might require the first six terms or more of the series expansion, for accurate results. Using these expansions, real-time computation becomes inefficient because higher powers of complex numbers are involved for all the samples in the fault window.

The new proposed method for estimating fault location given in (48) does not calculate hyperbolic terms in real-time and is more efficient than the series-expansion method. The proposed computationally efficient method is accurate with fault-locating errors shorter than a half mile for long overhead lines or underground cables. The errors introduced result from line transposition. Because only a negative- or positive-sequence network is used, the proposed method is best suited for any length of overhead line or underground cable. Also, this method is not affected by fault resistance, loading conditions, system-impedance ratios, or system nonhomogeneity.

## V. APPENDIX

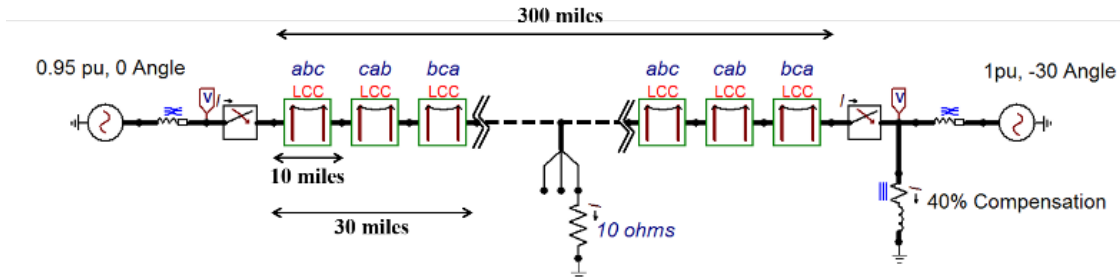Fig. 25 illustrates the system model used for simulation. Table I–Table III list the appropriate parameters.

**TABLE I**
**LOCAL AND REMOTE SOURCE PARAMETERS**

| Source Parameters | Local Source | Remote Source |
|---|---|---|
| Line-to-Line Voltage (kV) | $327.75\angle0°$ | $345\angle{-30°}$ |
| Total Positive-Sequence Impedance (Ω) | $72.02\angle84°$ | $35.59\angle65°$ |
| Total Zero-Sequence Impedance (Ω) | $230\angle77.47°$ | $129.59\angle65°$ |
| Frequency (Hz) | 60 | 60 |

**TABLE II**
**OVERHEAD LINE PARAMETERS FOR LCC BERGERON MODEL**

| Line Parameters | Values |
|---|---|
| Positive-Sequence Impedance per Mile (Ω) | $0.5876\angle88.13°$ |
| Zero-Sequence Impedance per Mile (Ω) | $1.5868\angle69.67°$ |
| Positive-Sequence Shunt Capacitance per Mile (nF) | 19.362 |
| Zero-Sequence Shunt Capacitance per Mile (nF) | 12.551 |
| Total Line Length (Miles) | 300 |
| Transposition Cycle (Miles) | 30 |
| Inner Radius of Phase Conductor (Inches) | 0 |
| Outer Radius of Phase Conductor (Inches) | 0.554 |
| DC Resistance of Phase Conductor per Mile (Ω) | 0.0215 |
| Number of Bundled Conductors per Phase | 2 |
| Inner Radius of Shield Conductor (Inches) | 0 |
| Outer Radius of Shield Conductor (Inches) | 0.1622 |
| DC Resistance of Shield Conductor per Mile (Ω) | 1.372 |
| Horizontal Tower Configuration in feet (A—B—C—Shield1—Shield2) | (0—24.5—49—8—41) |
| Vertical Tower Configuration in Feet (A—B—C—Shield1—Shield2) | (70—70—70—87.6—87.6) |
| Vertical Mid-Span Configuration in Feet (A—B—C—Shield1—Shield2) | (46.67—46.67—46.67—58.4—58.4) |
| Soil Resistivity (Ω – m) | 100 |
| Remote-Terminal Shunt-Reactor Inductance (H) | 3.0283 |



Fig. 25. ATPDraw system model used for simulations.

TABLE III
PERFECTLY TRANSPOSED UNDERGROUND CABLE PARAMETERS

| Line Parameters | Values |
|---|---|
| Positive-Sequence Impedance per Mile ($\Omega$) | $0.1328\angle72.93°$ |
| Zero- Sequence Impedance per Mile ($\Omega$) | $0.1914\angle26.03°$ |
| Positive-Sequence Shunt Capacitance per Mile (nF) | 187.17 |
| Zero-Sequence Shunt Capacitance per Mile (nF) | 124.78 |
| Total Line Length (Miles) | 200 |
| Remote Terminal Shunt Reactor Inductance (H) | 0.2 |

## VI. REFERENCES

[1] K. Zimmerman and D. Costello, "Impedance-Based Fault Location Experience," proceedings of the 58th Annual Conference for Protective Relay Engineers, College Station, TX, April, 2005.

[2] IEEE Standard C37.114-2014, IEEE Guide for Determining Fault Location on AC Transmission and Distribution Lines, (Revision of IEEE Std C37.114-2004)

[3] J. J. Grainger and W.D. Stevenson, "Current and Voltage Relations on a Transmission Line," *Power System Analysis*. Tata McGraw Hill, New Delhi, India, 2012, pp. 193–215.

[4] R. Abboud, W. F. Soares, and F. Goldman. "Challenges and Solutions in the Protection of a Long Line in the Furnas System," proceedings of the 32nd Annual Western Protective Relay Conference, Spokane, WA, October 2005.

[5] Y. Gong, M. Mynam, A. Guzmán, G. Benmouyal, and B. Shulim, "Automated Fault Location System for Nonhomogeneous Transmission Networks," proceedings of the 65th Annual Conference for Protective Relay Engineers, College Station, TX, April 2012.

[6] M. M. Saha, J. Izykowski, and E. Rosolowski, "Two-end and Multi-end Fault-location Algorithms," *Fault Location on Power Networks*. Springer, London, NY, 2010, pp. 300-309.

[7] S. E. Zocholl, "Three-Phase Circuit Analysis and the Mysterious $k_0$ Factor," proceedings of the 48th Annual Conference for Protective Relay Engineers, College Station, Texas, April, 1995.

[8] B. Kasztenny, H. J. Altuve, B. Le, and N. Fischer, "Tutorial on Fault Locating Embedded in Line Current Differential Relays – Methods, Implementation, and Application Considerations," proceedings of the 17th Annual Georgia Tech Fault and Disturbance Analysis Conference, Atlanta, GA, April 2014.

[9] D. Uznanski, "Series Expansion," *WolframMathWorld*, created by Eric W. Weisstein, 2018. Available: http://mathworld.wolfram.com/SeriesExpansion.html.

## VII. BIOGRAPHIES

**Kanchanrao Dase** received a B.E degree in electrical engineering from Sardar Patel College of Engineering, University of Mumbai in 2009. He received a M.S. degree in electrical engineering from Michigan Technological University, USA in 2015. From 2009 to 2014, he was a manager at Reliance Infrastructure Ltd. Mumbai Transmission Business with a substation engineering and commissioning profile. Currently, he is working with Schweitzer Engineering Laboratories Inc. as a Power Engineer. He has co-authored conference papers based on experiences of implementing IEC 61850 SCADA and teleprotection using SDH. His research interest includes power system protection, substation automation, and fault locating.

**Normann Fischer** received a Higher Diploma in Technology, with honors, from Technikon Witwatersrand, Johannesburg, South Africa, in 1988; a BSEE, with honors, from the University of Cape Town in 1993; an MSEE from the University of Idaho in 2005; and a PhD from the University of Idaho in 2014. He joined Eskom as a protection technician in 1984 and was a senior design engineer in the Eskom protection design department for three years. He then joined IST Energy as a senior design engineer in 1996. In 1999, Normann joined Schweitzer Engineering Laboratories, Inc., where he is currently a fellow engineer in the Research and Development division. He was a registered professional engineer in South Africa and a member of the South African Institute of Electrical Engineers. He is currently a senior member of IEEE and a member of the American Society for Engineering Education (ASEE).